Stability properties of a MIMO data flow controller

Ramón A. Delgado, Torbjörn Wigren, Katrina Lau and Richard H. Middleton

***Abstract*— The increasing demand for data in mobile applications has created a need for better communications systems. To satisfy this growing data demand next generation wireless systems are planned to use millimetre wave carrier frequencies. At these frequencies, radio shadowing is severe. To compensate for shadowing, incoming data flows must therefore be split and sent over several radio interfaces, that may have different delay properties. This paper analyses the stability properties of a MIMO data splitter that controls the delay skew between the data paths. The stability analysis is performed using IQC stability theory.**

***Index Terms*— Control of networks, stability of nonlinear systems.**

I. INTRODUCTION

Fifth generation (5G) wireless systems are expected to support several high-performance applications such as automotive safety, remote surgery and networked feedback control over wireless networks [1]. These applications require a wireless communication system with low latency and a constant sampling rate. Violation of these requirements may have severe consequences on performance and stability, as discussed in [2]. Current mobile broadband services have delays of tens of milliseconds, and large delay variations may occur. This fact makes them unsuitable for these new high-performance applications.

5G wireless networks will operate at millimetre wave carrier frequencies. At these frequencies, radio wave propagation has a beam-like behaviour where radio shadowing may be significant [1], [3]. The use of multi-point transmission may mitigate the effects of radio shadowing. Multi-point transmission increases the overall stability of the link by splitting incoming data into several data streams. These data streams are sent using multiple transmission nodes and are received at the other side of multiple wireless interfaces. The delays experienced by each data path may vary depending on the infrastructure and technologies used to transmit each data stream. Excessive delay skew in split flows can create problems with IP protocols, out of sequence packets, packet discard and retransmission. Thus, the delay skew between data streams needs to be controlled to reduce the delay variation in the presence of radio shadowing.

In [4] an algorithm for control of delay skew between data paths has been proposed. This algorithm uses the data queues at the transmission nodes as actuators to control the downlink delay experienced by each data path. The present paper responds to the recently released call for more research on delays in networked control [5]. The main contribution of the paper is a multiple input multiple output (MIMO) stability analysis of the delay skew controller presented in [4]. The stability analysis is performed using Integral Quadratic Constraints (IQC) theory [6].

Reference [4] and the current paper are part of an effort to tackle several delay control problems that arise in 4G and 5G wireless mobile communication networks. Related papers in this effort include [2], [4], [7], [8], [9]. In [8] the single input single output (SISO) inner loop used in this paper is described and analysed. Reference [7] describes an n-node round trip time skew control algorithm for critical machine type communications. As is pointed out in [2], regulation of round trip time skew is relevant in critical machine type communications, such as feedback control loops operating over wireless networks. On the other hand, regulation of downlink delay skew is relevant in applications such as augmented reality, where the data-rate in the uplink is much less than the data-rate in downlink. The stability analysis in [7] combines IQC theory and high-order Padé approximations to provide a stability limit, in terms of the maximum allowed round trip loop delay. The main three aspects in which this paper differs from the work of [7] are (i) the control loop configuration, i.e. the block diagram, dynamics and the location of the nonlinear components in the loop, (ii) the handling of the time delays as operator components in the IQC theory instead of replacing them with their Padé approximations, and (iii) the control objective that aims at controlling the downlink delay rather than the round trip delay. The paper [2] also treats a round trip delay skew control objective for the special case of two data paths. In this case, the stability problem is analysed by a combination of the SISO Nyquist and Popov criteria. The paper [9] analyses stability for the case of two data paths as well, but for the downlink delay skew control objective. The paper [4] is not focused on stability. It rather analyses the sensitivity and disturbance rejection properties of the algorithm of this paper, in order to provide general guidelines for the design of the networked data flow control system. The present paper is thus restricted to stability analysis. Numerical results illustrating the performance of the proposed delay skew controller are available in [4].

The notation uses boldface characters to denote vectors and matrices. Dynamics are represented in the Laplace transform as a function of the Laplace variable s. When handling nonlinear dynamics, a switch to the time domain is required. Time domain signals are represented with an

R.A Delgado, K. Lau and R.H. Middleton are with the School of Electrical Engineering and Computing, University of Newcastle, Australia {ramon.delgado, k.lau, richard.middleton}@newcastle.edu.au

T. Wigren is with L5GR Systems, Ericsson AB, Stockholm, SE-16480 Sweden torbjorn.wigren@ericsson.com

Peer-reviewed author's copy of:
R. A. Delgado, T. Wigren, K. Lau and R. H. Middleton. **Stability properties of a MIMO data flow controller**. In *2018 Annual American Control Conference (ACC)*, Milwaukee, WI, USA, 2018, pp. 2638-2643.
Available at https://doi.org/10.23919/ACC.2018.8431500

inverted caret as $\check{f}(t)$ where (t) indicates a dependence on the time variable.

The paper is organised as follows: Section II presents some motivating applications for the delay skew control problem. Section III introduces the networked control architecture. The stability analysis is described in section IV. Section V presents a numerical example. Finally, conclusions are drawn in section VI.

II. Delay Skew Control for 5G Applications

To motivate the work further some remarks on applications and corresponding requirements are in order. To put these remarks in the right context, the practical implementation of the block diagram of Fig. 1 needs to be discussed.

The networked control system of Fig. 1 is distributed over a data split node, multiple network interfaces and wireless transmission nodes, each transmitting over its separate air interface to the application. The applications of interest here are not subject to feedback control in the data split node as in [2], rather the applications are concerned with the display of the received data. A first important such case is where operators at industrial assembly lines are supported by streaming video that is overlayed on top the normal visual information. This overlayed video information could e.g. display 3D blueprints or instructions about the ongoing assembly. Another typical case concerns synchronisation of video shown on a large public screen, but where viewers obtain high fidelity audio in their headsets to reduce disturbances.

As stated in the introduction, millimetre wave carrier frequencies will entail use of multipoint transmission. The incoming application data is then split, for transmission from multiple base stations (transmission nodes). Depending on the circumstances, the data to each transmission node may be sent over network interfaces implemented with different technologies, like copper wire, optical fibre or wireless backhaul. This is one reason why the delay from the data split node to the wireless interfaces may be different over different paths. Other reasons for this include a varying network interface delay because of data traffic variations and the variation of the transmission queue dwell times caused by the rapidly varying radio fading [1]. The above two example applications lead to the control objectives of the present paper, namely to keep the delay skews between different transmission paths as low as possible, at the same time as the delay is kept constant. If this is unsuccessful, re-ordering buffers in the receiver of the application node may overflow and synchronisation of audio and video may experience noticeable variations.

In the implementation of Fig. 1, both the outer- and inner-loop controllers are located in the data split node, while the transmission nodes measure the downlink network interface delays, implements the transmission queues and measure their associated dwell times. The network interfaces transport the control- and feedback information needed for delay skew control.

III. Delay Skew Control

This section reviews the controller that regulates the downlink delay skew between multiple data paths.

The control scheme was presented in [9] for the two data path case with the $n+1$-data path version treated in [4]. In this section, the aspects of the networked data flow controller that are relevant for the IQC stability analysis are described. Fig. 1 shows a block diagram of the MIMO downlink delay skew controller. Cascade control is used, with a MIMO outer loop controller regulating the delay skew between the data paths and there are $n+1$ SISO inner loops controlling the queue dwell times. The assumptions under which the control scheme described in [4] is equivalent to the block diagram in Fig. 1 are described in this section.

The skew controller $\mathbf{C}_{skew}(s)$ in Fig. 1 is located in the node where the data is split into multiple flows. The delay skew control channels regulate $\mathbf{T}_{skew}(s)$ to follow a reference signal $\mathbf{T}^{ref}_{skew}(s)$. One of the data paths is selected as the reference path and this data path is associated with a delay sum control channel. Thus, the outer loop is composed of one delay sum control channel and n delay skew control channels. Then, $\mathbf{T}_{skew}(s)$ and $\mathbf{T}^{ref}_{skew}(s)$ are given by

$$\mathbf{T}_{skew}(s) = \begin{pmatrix} T_{skew,1}(s) & \cdots & T_{skew,n}(s) & T_{sum}(s) \end{pmatrix}^T \quad (1)$$

$$\mathbf{T}^{ref}_{skew}(s) = \begin{pmatrix} T^{ref}_{skew,1}(s) & \cdots & T^{ref}_{skew,n}(s) & T^{ref}_{sum}(s) \end{pmatrix}^T \quad (2)$$

where $T^{ref}_{skew,i}(s)$ for $i = 1, \ldots, n$ are the reference signals of the skew control channels, and $T^{ref}_{sum}(s)$ sets the total delay budget available to be distributed between the $n+1$ data paths. The network interface uses some of this budget, but the remaining delay budget is available for distribution between the transmission node queues of the data streams. The total delay budget should be high enough to ensure that the control problem is feasible.

In Fig. 1 matrices $\mathbf{M}$ and $\mathbf{F}$ have been used in [7] to perform static decoupling in the outer loop. Thus, the matrices $\mathbf{M}$ and $\mathbf{F}$ are given by

$$\mathbf{F} = \begin{pmatrix} 1 & 0 & 0 & 0 & -1 \\ 0 & \ddots & \ddots & \vdots & \vdots \\ \vdots & \ddots & 1 & 0 & -1 \\ 0 & \cdots & 0 & 1 & -1 \\ 1 & \cdots & 1 & 1 & 1 \end{pmatrix} \quad (3)$$

and

$$\mathbf{M} = \frac{1}{n+1} \begin{pmatrix} n & -1 & \cdots & \cdots & -1 & 1 \\ -1 & n & -1 & \cdots & -1 & 1 \\ \vdots & \ddots & \ddots & \ddots & -1 & 1 \\ \vdots & \vdots & \ddots & \ddots & -1 & 1 \\ -1 & \cdots & \cdots & -1 & n & 1 \\ -1 & \cdots & \cdots & \cdots & -1 & 1 \end{pmatrix}. \quad (4)$$

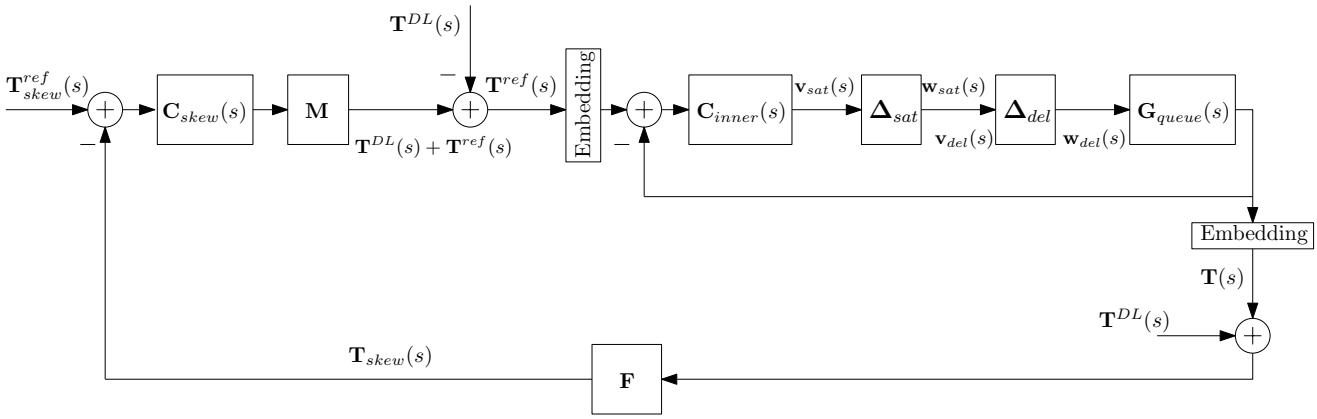

Fig. 1. Block diagram used in the IQC stability analysis.

By using this decoupling strategy, the MIMO skew controller $\mathbf{C}_{skew}(s)$ can be selected as follows

$$\mathbf{C}_{skew}(s) = \begin{pmatrix} C_{skew,1}(s) & 0 & 0 & 0 \\ 0 & \ddots & 0 & \vdots \\ \vdots & \ddots & C_{skew,n}(s) & 0 \\ 0 & 0 & 0 & C_{sum}(s) \end{pmatrix}.$$

A. Inner loop

The inner loop controller $\mathbf{C}_{inner}(s)$ regulates the volume of data in $n+1$ queues. Here a brief description of the inner loop is given, more detailed descriptions of the inner loop and its applications can be found in [4], [8], [9].

The inner loop output is given by

$$\mathbf{T}(s) = \begin{pmatrix} T_1(s) & \cdots & T_n(s) & T_r(s) \end{pmatrix}^T \tag{5}$$

where $T_i(s)$ for $i = 1, \ldots, n$ are the queue dwell time signals for n-queues, and $T_r(s)$ is queue dwell time of the reference path. The inner loop reference signal $\mathbf{T}^{ref}(s)$ is defined in a similar manner. In Fig. 1 the inner loop controller $\mathbf{C}_{inner}(s)$ determinates the data volume that is sent to each queue. To incorporate the fact that the network interfaces have limited capacity, and that the packets in the downlink are not sent in the uplink direction, a saturation is included in each inner loop. The block $\mathbf{\Delta}_{sat}$ models the effect of the saturations introduced in the inner loops as follows

$$\mathbf{\Delta}_{sat}\check{\mathbf{v}}_{sat}(t) = \begin{pmatrix} sat_1(\check{v}_{sat,1}(t)) & 0 & 0 & 0 \\ 0 & \ddots & 0 & 0 \\ 0 & 0 & sat_n(\check{v}_{sat,n}(t)) & 0 \\ 0 & 0 & 0 & sat_r(\check{v}_{sat,r}(t)) \end{pmatrix}$$

where

$$\check{\mathbf{v}}_{sat}(t) = \begin{pmatrix} \check{v}_{sat,1}(t) & \cdots & \check{v}_{sat,n}(t) & \check{v}_{sat,r}(t) \end{pmatrix}^T \tag{6}$$

is the input of the $\mathbf{\Delta}_{sat}$ block and $sat_i(\cdot)$ for $i = 1, \ldots, n, r$ is given by

$$sat_i(\check{u}(t)) = \begin{cases} u_{max} & if \quad \check{u}(t) > u_{max} \\ \check{u}(t) & if \quad 0 \le \check{u}(t) \le u_{max} \\ 0 & if \quad \check{u}(t) < 0. \end{cases} \tag{7}$$

The block $\mathbf{\Delta}_{del}$ in Fig. 1 accounts for the uplink and downlink delays, i.e.

$$\mathbf{\Delta}_{del}\check{\mathbf{v}}_{del}(t) = \begin{pmatrix} \check{v}_{del,1}(t - \check{\tau}_1(t)) & 0 & 0 & 0 \\ 0 & \ddots & 0 & 0 \\ 0 & 0 & \check{v}_{del,n}(t - \check{\tau}_n(t)) & 0 \\ 0 & 0 & 0 & \check{v}_{del,r}(t - \check{\tau}_r(t)) \end{pmatrix}$$

where $\check{\tau}_i(t) = \check{T}^{DL}_i(t) + T^{UL}_i$ and the input of $\mathbf{\Delta}_{del}$ block is given by

$$\check{\mathbf{v}}_{del}(t) = \begin{pmatrix} \check{v}_{del,1}(t) & \cdots & \check{v}_{del,n}(t) & \check{v}_{del,r}(t) \end{pmatrix}^T. \tag{8}$$

The block $\mathbf{\Delta}_{del}$ models the effect of the uplink and downlink delays. To combine the effects of the uplink and downlink delays into $\mathbf{\Delta}_{del}$ it is assumed that the uplink delays are time invariant. Thus, the following assumption is assumed to hold

A1) The uplink delays T^{UL}_i, $i = 1, \ldots, n, r$ are time invariant.

As explained in [4], this assumption is reasonable at least in the case when there is no congestion in the uplink. The outer loop thus treats the uplink delays as constant signals, but it treats the downlink delays as dynamic signals.

The inner loop controller $\mathbf{C}_{inner}(s)$ regulates data volume, but the reference signal for the inner loop, $\check{\mathbf{T}}^{ref}(t)$ is provided in terms of the dwell time. Thus, a transformation from a dwell time reference signal to a data volume reference signal is needed. This transformation is accomplished by multiplying each dwell time reference value $\check{T}^{ref}_i(t)$ by the scheduled wireless data rate $\check{w}_{air,i}(t)$. Consistently, the queue dwell time $\check{T}_i(t)$ is obtained by dividing the queue data volume by the corresponding scheduled wireless data rate. Next, it needs to be assumed that the embedding described above is working as planned. This embedding allows neutralizing the effect of $\check{w}_{air,i}(t)$ at the input and output of the inner loop. Assumptions A2 and A3 are introduced for this purpose, cf. [4].

A2) The bandwidth of $\check{w}_{air,i}(t)$ is significantly higher than the bandwidth of $\check{T}^{ref}_i(t)$ for $i = 1, \ldots, n, r$. The following relations therefore hold

1) $(\check{w}_{air,i}(t))^{-1} \approx (\bar{w}_{air,i})^{-1}$, $i = 1, \ldots, n, r$, where $\bar{w}_{air,i}$ is the is the average over time of the scheduled bit rates.
2) $\mathcal{L}\left(\check{T}_i^{ref}(t)\check{w}_{air,i}(t)\right) \approx T_i^{ref}(s)\bar{w}_{air,i}$, $i = 1, \ldots, n, r$.

A3) The inner loops operate as intended, with data flow rate saturation being inactive.

Note that A3 is only assumed to cancel the effect of the embedding. The rate saturations are fully retained in the IQC analysis that follows below. Additionally, $\mathbf{G}_{queue}(s)$ represents the MIMO model of the queues, i.e.

$$\mathbf{G}_{queue}(s) = \begin{pmatrix} \frac{1}{s+\delta_1} & 0 & 0 & 0 \\ 0 & \ddots & 0 & \vdots \\ \vdots & \ddots & \frac{1}{s+\delta_n} & 0 \\ 0 & 0 & 0 & \frac{1}{s+\delta_r} \end{pmatrix}. \quad (9)$$

where the leakage factor $\delta_i > 0, i = 1, \ldots, n, r$ indicates that Active Queue Management (AQM) [10], [8] is used, with AQM intentionally discarding some packets in the queues. The inner loop controllers are now included in a diagonal MIMO controller $\mathbf{C}_{inner}(s)$ as follows

$$\mathbf{C}_{inner}(s) = \begin{pmatrix} C_1(s) & 0 & 0 & 0 \\ 0 & \ddots & 0 & \vdots \\ \vdots & \ddots & C_n(s) & 0 \\ 0 & 0 & 0 & C_r(s) \end{pmatrix}. \quad (10)$$

B. MIMO model for stability analysis

A prerequisite for the IQC stability analysis is to turn the block diagram in Fig. 1 into a standard representation. In [7] a similar approach was used. However, in [7], the control objective, inner loops and external signals were different. Hence a modified variant of the model is needed here. The IQC stability analysis is performed on a system having the following representation

$$\begin{aligned} \mathbf{v}(s) &= \mathbf{G}(s)\mathbf{w}(s) + \mathbf{x}(s) & (11) \\ \check{\mathbf{w}}(t) &= \mathbf{\Delta}\check{\mathbf{v}}(t). & (12) \end{aligned}$$

$\mathbf{G}(s)$ is a rational transfer function matrix with no poles in the right complex half plane. $\mathbf{\Delta}$ denotes a bounded causal operator, while $\mathbf{x}(s)$ denotes an external vector signal. $\mathbf{v}(s)$ and $\mathbf{w}(s)$ denote the two internal vector signals.

The vector signal $\mathbf{v}(s)$ is given by

$$\mathbf{v}(s) = \begin{pmatrix} \mathbf{v}_{del}(s)^T & \mathbf{v}_{sat}(s)^T \end{pmatrix}^T \quad (13)$$

where $\mathbf{v}_{del}(s)$ and $\mathbf{v}_{sat}(s)$ are defined in (8) and (6), respectively. Analogously, the signal $\mathbf{w}(s)$ is given by

$$\mathbf{w}(s) = \begin{pmatrix} \mathbf{w}_{del}(s)^T & \mathbf{w}_{sat}(s)^T \end{pmatrix}^T \quad (14)$$

where

$$\begin{aligned} \mathbf{w}_{del}(s) &= \begin{pmatrix} w_{del,1}(s) & \cdots & w_{del,n}(s) & w_{del,r}(s) \end{pmatrix}^T & (15) \\ \mathbf{w}_{sat}(s) &= \begin{pmatrix} w_{sat,1}(s) & \cdots & w_{sat,n}(s) & w_{sat,r}(s) \end{pmatrix}^T & (16) \end{aligned}$$

are the outputs of the blocks $\mathbf{\Delta}_{del}$ and $\mathbf{\Delta}_{sat}$. The quantities of (13)-(16) appear in Fig. 1.

The operator $\mathbf{\Delta}$ accounts for the saturation and the delays in the inner loops. Thus, the bounded causal operator $\mathbf{\Delta}$ is composed as follows

$$\mathbf{\Delta}\check{\mathbf{v}}(t) = \begin{pmatrix} \mathbf{\Delta}_{sat}\check{\mathbf{v}}_{sat}(t) & \mathbf{0} \\ \mathbf{0} & \mathbf{\Delta}_{del}\check{\mathbf{v}}_{del}(t) \end{pmatrix} \quad (17)$$

The causal operators $\mathbf{\Delta}_{sat}$ and $\mathbf{\Delta}_{del}$ are suitable for analysis using IQC theory, with $\mathbf{\Delta}_{sat}$ representing a collection of memoryless sector nonlinearities and $\mathbf{\Delta}_{del}$ describing a collection of uncertain time delays.

Next, to describe the loop in the block diagram in Fig. 1 in the form of (11)-(12) the rational transfer function matrix $\mathbf{G}(s)$ and the vector signal $\mathbf{x}(s)$ are defined as follows

$$\mathbf{G}(s) = \begin{pmatrix} \mathbf{0} & -\mathbf{C}_{inner}(s)(\mathbf{M}\mathbf{C}_{skew}(s)\mathbf{F} + \mathbf{I})\mathbf{G}_{queue}(s) \\ \mathbf{I} & \mathbf{0} \end{pmatrix} \quad (18)$$

$$\begin{aligned} \mathbf{x}(s) &= \begin{pmatrix} \mathbf{x}_1(s) \\ 0 \end{pmatrix} \\ \mathbf{x}_1(s) &= \mathbf{C}_{inner}(s)\mathbf{M}\mathbf{C}_{skew}(s)\mathbf{T}_{skew}^{ref}(s) \\ &\quad -\mathbf{C}_{inner}(s)(\mathbf{M}\mathbf{C}_{skew}(s)\mathbf{F} + \mathbf{I})\mathbf{T}^{DL}(s) \end{aligned}$$

where

$$\mathbf{T}^{DL}(s) = \begin{pmatrix} T_1^{DL}(s) & \cdots & T_n^{DL}(s) & T_r^{DL}(s) \end{pmatrix}^T. \quad (19)$$

The block diagram of Fig. 1 is now in the form of (11)-(12) required by the IQC analysis described in the following section.

IV. IQC STABILITY ANALYSIS

This section presents an IQC stability analysis of the system defined in the previous section. The first step in the analysis is to review the basic tools and definitions used in IQC theory [6]. Next, assumptions on the components of the delay skew control scheme of Fig. 1 are introduced. Finally, the main result in IQC theory [6] is used to formulate Theorem 1.

A. Tools of Analysis

The following definitions of [6], [11] are needed to set up the framework for the IQC analysis.

Definition 1: $\mathcal{L}_2^m$ denotes the space of $\mathcal{R}^m$-valued functions $\check{\mathbf{f}}(\cdot) : [0, \infty) \to \mathcal{R}^m$ of finite energy, i.e.

$$\left\|\check{\mathbf{f}}(\cdot)\right\|^2 = \int_0^\infty \check{\mathbf{f}}^T(t)\check{\mathbf{f}}(t)dt < \infty. \quad (20)$$

Definition 2: The space $\mathcal{L}_{2e}^m$ is an extension of the space $\mathcal{L}_2^m$, whose members are $\mathcal{R}^m$-valued functions $\check{\mathbf{f}}(\cdot) : [0, \infty) \to \mathcal{R}^m$, such that their time truncation

$$\check{\mathbf{f}}_T(t) = \begin{cases} \check{\mathbf{f}}(t), & 0 \le t \le T \\ \mathbf{0}, & t > T \end{cases} \in \mathcal{L}_2^m. \quad (21)$$

Definition 3: The feedback interconnection of $\mathbf{G}(s)$ and $\mathbf{\Delta}$ as in (11)-(12) is *well-posed* if it defines a causal map $\check{\mathbf{x}}(\cdot) \to (\check{\mathbf{v}}(\cdot), \check{\mathbf{w}}(\cdot))$ on $\mathcal{L}_{2e}^m$, i.e. for any $\check{\mathbf{x}}(\cdot) \in \mathcal{L}_{2e}^m$ there exists a solution $(\check{\mathbf{v}}(\cdot), \check{\mathbf{w}}(\cdot))$ that depends causally on $\check{\mathbf{x}}(\cdot)$.

The interconnection is *stable* if, in addition, the inverse is bounded. This means that there exists a constant $C_{IQC} > 0$ such that

$$\int_0^T (\check{\mathbf{v}}^T(t)\check{\mathbf{v}}(t) + \check{\mathbf{w}}^T(t)\check{\mathbf{w}}(t))dt \leq C_{IQC} \int_0^T \check{\mathbf{x}}^T(t)\check{\mathbf{x}}(t)dt. \tag{22}$$

In the rest of the paper, the superscript m in $\mathcal{L}_{2e}^m$ will be omitted.

A bounded operator $\mathbf{\Delta}$ is said to satisfy the IQC defined by $\mathbf{\Pi}$, if for all $\mathbf{v}, \mathbf{w}$

$$\int_{-\infty}^{\infty} \begin{bmatrix} \mathbf{v}(j\omega) \\ \mathbf{w}(j\omega) \end{bmatrix}^H \mathbf{\Pi}(j\omega) \begin{bmatrix} \mathbf{v}(j\omega) \\ \mathbf{w}(j\omega) \end{bmatrix} d\omega \geq 0 \tag{23}$$

with $\check{\mathbf{w}}(t) = \mathbf{\Delta}\check{\mathbf{v}}(t)$. The matrix $\mathbf{\Pi}$ denotes the multiplier defining the IQC.

Next assume that the following conditions hold:

- C1) $\mathbf{G}(s)$ is a proper rational function with real coefficients and without poles in the closed right half-plane.
- C2) The interconnection of $\mathbf{G}(s)$ and $\tau\mathbf{\Delta}$ is well posed for all $\tau \in [0, 1]$.
- C3) For $\mathbf{x}(s)$ as in (11), $\check{\mathbf{x}}(\cdot) \in \mathcal{L}_{2e}$.
- C4) $\mathbf{\Delta}$ is a bounded causal operator.
- C5) $\tau\mathbf{\Delta}$ satisfy the IQC defined by $\mathbf{\Pi}$.

The main result in IQC theory is then:

Lemma 1 ([6]): Assume that C1-C5 hold. If there exists $\epsilon > 0$ such that $\forall\omega \in \mathcal{R} \cup \{\infty\}$

$$\begin{bmatrix} \mathbf{G}(j\omega) \\ I \end{bmatrix}^H \mathbf{\Pi}(j\omega) \begin{bmatrix} \mathbf{G}(j\omega) \\ I \end{bmatrix} \leq -\epsilon I, \tag{24}$$

then, the feedback interconnection of $\mathbf{G}(s)$ and $\mathbf{\Delta}$ of (11)-(12) is stable.

A summary giving an intuitive explanation of C1-C5 appears in [7], c.f. [6] and [11].

B. Assumptions on the delay skew controller

In addition to assumptions A1-A3, the following assumptions are required for the IQC analysis of the delay skew controller.

- A4) $\delta_i > 0$, $i = 1, \ldots, n, r$ and the transfer functions $C_{sum}(s)$, $C_r(s)$, $C_{skew,i}(s)$ and $C_i(s)$, $i = 1, \ldots, n$ are proper rational transfer functions without poles in the closed right complex half-plane.
- A5) $\check{\mathbf{T}}_{skew}^{ref}(\cdot), \check{\mathbf{T}}^{DL}(\cdot) \in \mathcal{L}_{2e}$.
- A6) The interconnection of $\mathbf{G}(s)$ and $\tau\mathbf{\Delta}$ is well posed for every $\tau \in [0, 1]$.

Assumption A4 ensures that $\mathbf{G}(s)$ is a proper rational transfer function with real coefficients without poles in the right half-plane. The assumption that $\delta_i > 0$ for $i = 1, \ldots, n, r$ indicates that Active Queue Management [10] is used in the inner loops. The assumption on the location of the poles of the controllers indicates that such controllers must be open loop stable.

C. Verification of IQC conditions

Before applying the IQC result described in Lemma 1 it is necessary to verify that assumptions A1-A6 imply that C1-C5 hold. Condition C1 follows from (18) if $\mathbf{C}_{skew}(s)$, $\mathbf{C}_{inner}(s)$ and $\mathbf{G}_{queue}(s)$ are proper rational transfer functions without poles in the closed right half-plane. Then, assumption A4 ensures that C1 holds. Assumption A4 also ensures that $\mathbf{C}_{skew}(s)$ and $\mathbf{C}_{inner}(s)$ are bounded operators, thus A4-A5 make sure that condition C3 is met. From the analysis in [6], [11] it is well known that conditions C4-C5 are satisfied by the bounded operators considered in the current paper.

Assumptions A1-A3 are needed to represent the cascade block diagram in Fig. 1 into the representation (11)-(12) used for IQC stability analysis. Assumption A3 was made with the purpose to make the embedding in Fig. 1 possible and not with the purpose to ignore the sector nonlinearities in the stability analysis. These nonlinearities are now included in the stability analysis to give the following result.

Theorem 1: Consider the feedback interaction of (11)-(12) and assume that the conditions A1-A6 hold. Suppose that $\mathbf{\Delta}$ of (17) satisfy the IQC given by $\mathbf{\Pi}$. Then, the feedback interconnection (11)-(12) is stable if there exists $\epsilon > 0$ such that (24) holds $\forall\omega \in \mathcal{R} \cup \{\infty\}$.

V. Numerical results

To illustrate the analysis above, numerical stability results are given. Proportional controllers are first chosen for the inner and outer loop. This choice of the controllers provides insights into the trade-offs in the controller design.

The IQC stability tests were performed using the IQC toolbox [12]. For the numerical analysis, it is assumed that a saturation satisfies the IQC of a sector nonlinearity and also the IQC given by the Popov multiplier. Stability is tested under the premise that each delay satisfies the IQCs for an uncertain time-invariant delay, see [6], [12]. In the representation of uncertain time delays in the simulations, the poles of the multipliers have been located at $a_1 = 0.01$ and $a_2 = 0.1$.

The IQC stability tests search for the largest round-trip delay, τ^*, which implies stability of the MIMO control loop. This value is computed by testing stability for each value of $\tau \in \{1ms, 2ms, 3ms, \ldots, 20ms\}$ and reporting as τ^* the maximum value of τ for which stability of the MIMO control loop is guaranteed.

First, consider the case in which there are three data paths, i.e. $n = 2$, that $\mathbf{C}_{skew}(s) = I_3$ and $\mathbf{C}_{inner}(s) = C_{inner}I_3$ where C_{inner} is a constant gain. Fig. 2 shows the maximum round trip delay, $\tau^* \in [1ms, 20ms]$, that guarantees stability as a function of C_{inner}. In Fig. 2 C_{inner} varies between 10 and 400. Note that when $C_{inner} \leq 70$ stability is guaranteed for $\tau \leq 20ms$.

Next, consider the case in which there are two data paths, i.e. $n = 1$, that $\mathbf{C}_{skew}(s) = C_{skew}(s)I_2$ and $\mathbf{C}_{inner}(s) =$

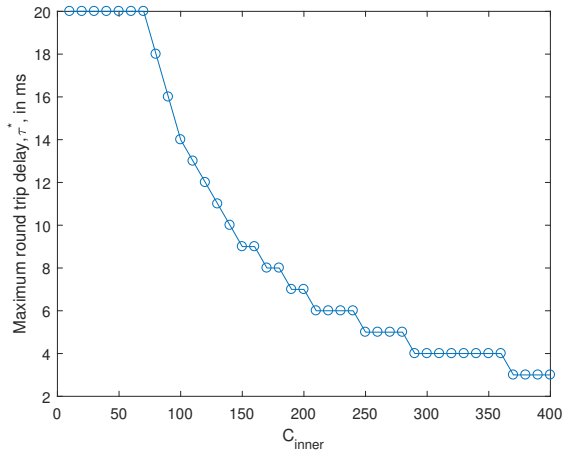

Fig. 2. Largest round trip delay which guarantees stability, $\tau^* \in [1ms, 20ms]$, as a function of C_{inner}.

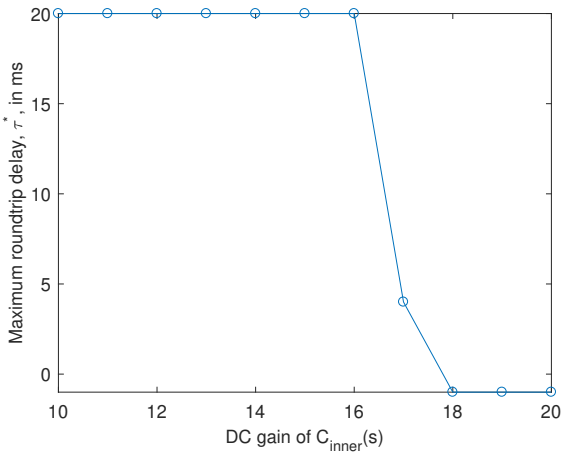

Fig. 3. Largest round trip delay which guarantees stability, $\tau^* \in [1ms, 20ms]$, as a function of the low-frequency gain of $C_{inner}(s)$.

$C_{inner}(s)I_2$ where

$$C_{skew}(s) = 0.1\,\frac{s+5.76}{10s+5.76}, \quad (25)$$

$$C_{inner}(s) = \alpha\,\frac{0.22798(s+30.49)(s+2.3)}{(s+69.51)(s+0.23)}, \quad (26)$$

and α is the low-frequency gain of $C_{inner}(s)$, i.e. $\alpha = C_{inner}(0)$. Note that $C_{skew}(0) = 0.1$. The controllers in (25)-(26) have the poles and zeros used in [9], but the static gains are different. IQC stability tests were performed using $\alpha \in [10, 20]$. Fig. 3 shows τ^* as a function of α. The value $\tau = -1$ denotes that there is no stability guarantee. In Fig. 3 when $C_{inner}(0) \leq 16$ stability is guaranteed for $\tau \leq 20ms$, but if $C_{inner}(0) \geq 18$ then there is no stability guarantee using the IQC analysis proposed here. This result is explained by [3].

VI. CONCLUSION

The use of multi-point transmissions will compensate the adverse shadowing conditions at millimetre wave carrier frequencies encountered in 5G wireless systems. A synchronised arrival of originally adjacent data packets sent over these flows is crucial to the success of the multi-point transmission strategy. This paper analyses the stability of a recently proposed downlink delay skew controller. The stability analysis of this MIMO controller is performed using IQC theory. The numerical results are consistent with experimental test bed results reported in a companion paper and related publications.

ACKNOWLEDGEMENTS

This research was supported under Australian Research Council's Linkage Projects funding scheme (project number LP150100757).

REFERENCES

[1] T. S. Rappaport, R. W. H. Jr., R. C. Daniels, and J. N. Murdock, *Millimeter Wave Wireless Communications*. Prentice Hall, 2014.

[2] R. H. Middleton, T. Wigren, K. Lau, and R. A. Delgado, "Data flow delay equalization for feedback control application using 5G wireless dual connectivity," in *2017 IEEE 85th Vehicular technology Conference (VTC Spring)*, Sydney, Australia, June 2017.

[3] T. Wigren, "Low-frequency limitations in saturated and delayed networked control," in *2015 IEEE Conference on Control Applications (CCA)*, Sydney, Australia, Sep. 21-23 2015.

[4] K. Lau, T. Wigren, R. Delgado, and R. Middleton, "Disturbance rejection properties for a 5G networked data flow delay controller," in *2017 IEEE 56th Conference on Decision and Control (CDC)*, Melbourne, Australia, 2017.

[5] T. Samad, "Control systems and the internet of things," *IEEE Control Systems*, vol. 36, pp. 13–16, 2016.

[6] A. Megretski and A. Rantzer, "System analysis via integral quadratic constraints," *IEEE Transactions on Automatic Control*, vol. 42, no. 6, pp. 819–830, 1997.

[7] R. Delgado, K. Lau, R. H. Middleton, and T. Wigren, "Networked delay control for 5G wireless machine type communications using multi-connectivity," *to appear in IEEE Transactions on Control Systems Technology*, 2018.

[8] T. Wigren, "Robust $\mathcal{L}_2$ stable networked control of wireless packet queues over delayed internet connections," *IEEE Transactions on Control Systems Technology*, vol. 24, pp. 502–513, 2016.

[9] T. Wigren, K. Lau, R. A. Delgado, and R. H. Middleton, "Delay skew packet flow control in wireless systems with dual connectivity," *to appear in IEEE Transactions on Vehicular Technology*, 2018.

[10] R. Adams, "Active queue management: A survey," *IEEE Communications Surveys Tutorials*, vol. 15, pp. 1425–1476, 2013.

[11] C.-Y. Kao and A. Rantzer, "Stability analysis of systems with uncertain time-varying delays," *Automatica*, vol. 43, pp. 959–979, 2007.

[12] C.-Y. Kao, A. Megretski, U. T. Jonsson, and A. Rantzer, "A MATLAB toolbox for robustness analysis," in *Computer Aided Control Systems Design, IEEE International Symposium on*, Taipei, 2004, pp. 297–302.